

**Supporting Information for:**  
**Real-time *in situ* analysis of biocorona formation and  
evolution on silica nanoparticles in defined and  
complex biological environments**

Rickard Frost<sup>a,b,\*</sup>, Christoph Langhammer<sup>b</sup>, Tommy Cedervall<sup>c</sup>

<sup>a</sup> Department of Energy and Environment, Chalmers University of Technology,  
SE-412 96, Gothenburg, Sweden

<sup>b</sup> Department of Physics, Chalmers University of Technology,  
SE-412 96, Gothenburg, Sweden

<sup>c</sup> Biochemistry and Structural Biology and NanoLund, Lund University,  
Box 124, SE-221 00 Lund, Sweden

\*Corresponding Author:

Rickard Frost, e-mail: [rickard.frost@chalmers.se](mailto:rickard.frost@chalmers.se)

## Brief description of the Core-Shell Nanoplasmonic Sensors

The nanoplasmonic sensing methodology applied in this study was recently described in detail elsewhere (including e.g. fabrication and characterization of the core-shell nanostructures).<sup>1</sup> Here, we summarize the main characteristics of the sensors to aid the understanding of the present article.

The core-shell nanostructures were manufactured using a bottom-up nanofabrication methodology called “hole-mask colloidal lithography”<sup>2</sup> with a subsequent annealing step (800°C, 24 h) followed by the deposition of an oxide layer - here 10 nm SiO<sub>2</sub>. The annealing step was introduced to change the morphology of the Au nanostructures from truncated cones to faceted (Wulff-shaped) nanoparticles with predominantly (111) and (100) facets. In Figure S1 data on the dimensions and morphology of the Au-nanostructures, before and after annealing, are presented.

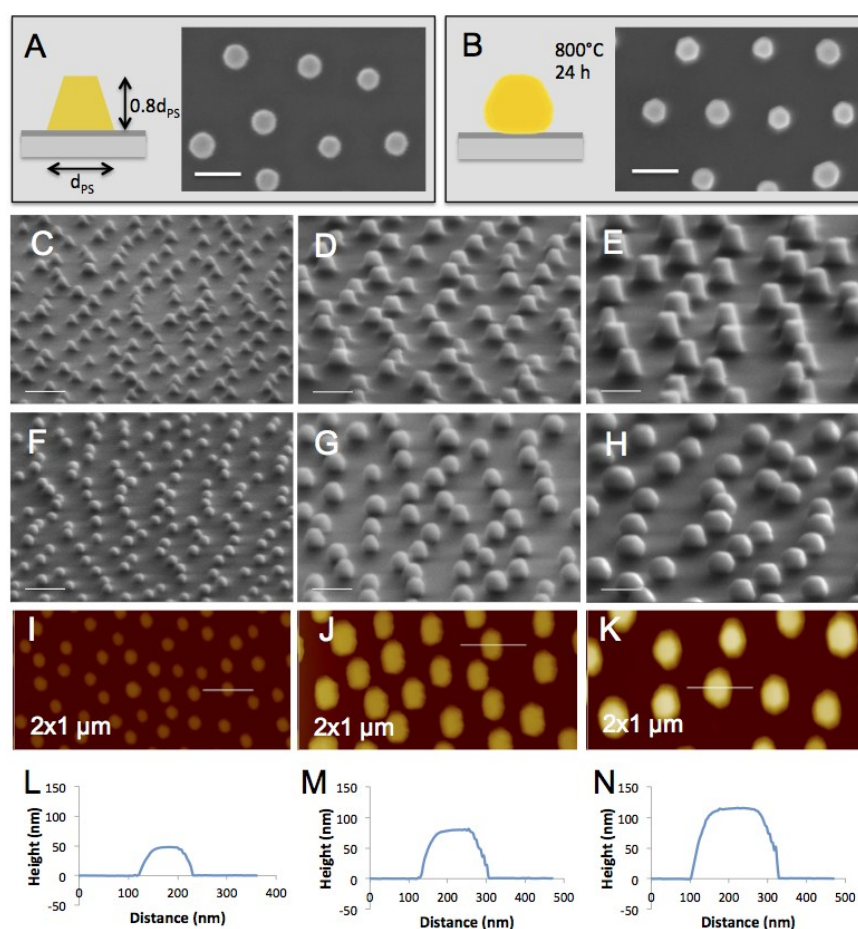


Figure S1. Schematic depiction of the Au-nanostructures (A) before and (B) after annealing in air (800°C, 24 h) together with corresponding top view SEM images (x100 000). Note the hexagonal faceting present after annealing (scale bars: 200 nm). (C-E) SEM images (x250 000, tilt 75°) showing the three different sizes and the shapes of the Au-nanostructures (C-E) before and (F-H) after thermal annealing (scale bars: 200 nm). (I-K) AFM images of the nanostructures shown in F-H and (L-N) corresponding cross sections. Reprinted with permission from (Frost, R.; Wadell, C.; Hellman, A.; Molander, S.; Svedhem, S.; Persson, M.; Langhammer, C. Core-Shell Nanoplasmonic Sensing for Characterization of Biocorona Formation and Nanoparticle Surface Interactions. *ACS Sensors* 2016, 1, 798-806.). Copyright (2016) American Chemical Society.

To characterize the core-shell structures after the deposition of 10 nm SiO<sub>2</sub> shell layer they were analyzed using TEM (Figure S2A-F). Based on the projected hexagonal shape of the core-shell nanostructures identified from the TEM images, the lengths of the flat (facets) and the curved regions were quantified, and a 2D and 3D model of their morphology was developed (Figure S2G).

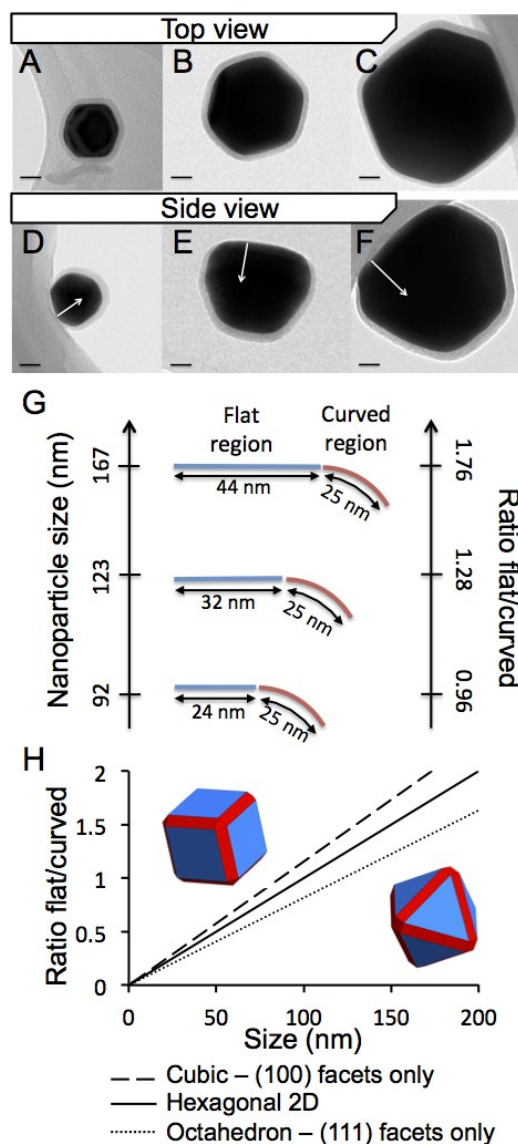


Figure S2. (A-F) To-scale TEM images, top and side views, of the three sizes of Au core - SiO<sub>2</sub> shell nanoparticles used in our study. In the side views the arrows point toward the top of the nanoparticles (i.e. away from the facet formerly in contact with the support). All scale bars equal 20 nm. (G) 2D model based on the projected hexagonal shape of the core-shell plasmonic sensing nanoparticles. Determined lengths of single flat and curved regions in the hexagonal structure, and calculated ratios thereof, for the different nanoparticle sizes. (H) Modeled ratios of cubic and octahedral Au-nanoparticles (in 3D) compared with the hexagonal 2D model. Reprinted with permission from (Frost, R.; Wadell, C.; Hellman, A.; Molander, S.; Svedhem, S.; Persson, M.; Langhammer, C. Core-Shell Nanoplasmonic Sensing for Characterization of Biocorona Formation and Nanoparticle Surface Interactions. *ACS Sensors* 2016, 1, 798-806.). Copyright (2016) American Chemical Society.

To compare the geometry of the faceted core-shell nanostructures described in Figure S2, with the size of the colloidal SiO<sub>2</sub> nanoparticles used in the second part of our

analysis reported in the main text, we further analyzed the obtained TEM images. By approximating circles to the surface curvature of the 2D projection of the core-shell nanostructures it is evident that the curvature at the edges between facets corresponds to a circle with a radius of about 26 nm (Figure S3). Therefore, colloidal silica nanoparticles with a similar radius were chosen for the DLS and SDS-PAGE experiments.

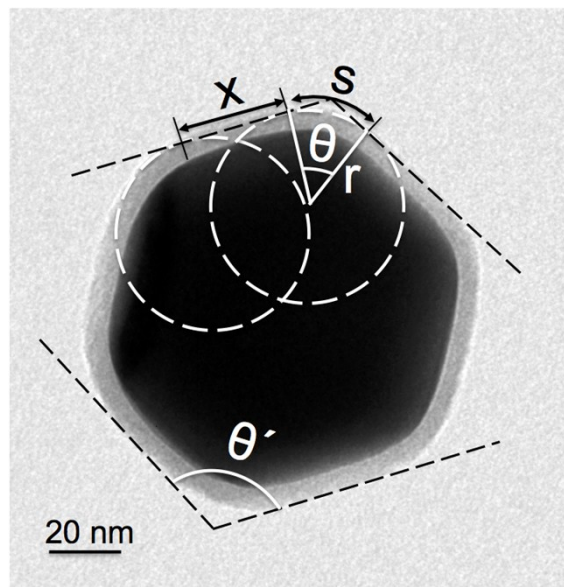


Figure S3. TEM image (top view) of a 123 nm Au core – SiO<sub>2</sub> shell nanoparticle with outlined geometry. The length of flat facets (X) and curved regions (S) are given in Figure S2. The radii of circles (r) with similar curvature as the curved regions of the nanoparticles were close to 26 nm. The indicated angles  $\theta$  and  $\theta'$  were determined to  $55\pm 3^\circ$  and  $120\pm 3^\circ$ , respectively.

## Experimental Section

Unless otherwise stated all chemicals were obtained from commercial sources and used without further purification. Deionized water was obtained from a Milli Q purification unit (Millipore, France) (resistivity 18.2 M $\Omega$ /cm). Phosphate buffered saline (PBS) was prepared from tablets (0.0015 M potassium dihydrogen phosphate, 0.0081 M disodium hydrogen phosphate, 0.0027 M potassium chloride and 0.137 M sodium chloride, pH 7.4) (Sigma Aldrich). Silica nanoparticles were obtained from Akzo Nobel (Bohus, Sweden). Bovine serum was obtained from Innovative Research and from Sigma Aldrich. Bovine serum albumin was obtained from Sigma Aldrich.

### *Purification of IgG from Bovine Serum*

IgG was purified from bovine serum using protein A/G sepharose, as previously described.<sup>3</sup> IgG depleted bovine serum was prepared by passing bovine serum over the protein A/G sepharose twice, as previously described.<sup>3</sup> This process, as judged by SDS-PAGE, removed about 90-95 % of the IgG in bovine serum. Bovine serum albumin and IgG were characterized by DLS and SDS-PAGE (not shown). The concentration of BSA was calculated from the weight of freeze dried protein and the concentration of IgG by using the extinction coefficient 1.38 at 280 nm.

### *Nanoplasmonic Sensing*

The fabrication and characterization of the three types of NPS surfaces are described in detail elsewhere<sup>1</sup> and in the SI. The NPS experiments were carried out in an XNano System (Insplorion AB, Sweden). Analysis of the LSPR response to derive the peak shift response was done by a MATLAB-based program fitting a Lorentzian function to the measured LSPR peak. Prior to use the sensors were treated by UV-ozone for >20 min. All experiments were carried out at room temperature. The PBS was degassed by sonication at low pressure before use to avoid formation of air bubbles in the system. Bovine serum and IgG depleted bovine serum were diluted x80 (to reach a final protein concentration of about 1 mg/mL) in PBS. IgG was diluted in PBS to a final concentration of 0.25 mg/mL. BSA was dissolved in PBS to a concentration of 1 mg/mL. The final dilutions in filtered and degassed PBS were performed right before use. A flow rate of 100  $\mu$ L/min was applied.

### *Corona Formation on Silica Nanoparticles in Dispersion*

The corona was formed by mixing silica nanoparticles in PBS with BSA, IgG, or bovine serum at indicated protein and particle concentrations. The mixture was incubated for 1 hour at room temperature before continuing with size measurements, protein analysis or protein exchange experiments. To observe the formation of the corona on particles on which a BSA corona already had been formed, the BSA incubated silica particles were mixed with IgG or bovine serum at indicated concentrations and incubated for at least 1h at room temperature. Subsequently, the size of the formed complexes and the adsorbed proteins were characterized by DLS and SDS-PAGE, respectively. To analyze the adsorbed proteins, the silica particles incubated in BSA, IgG, and/or bovine serum were first centrifuged for 10 min at 13000 rpm. After centrifugation the supernatant was discarded. To avoid proteins not adsorbed to the silica particles the pellets were washed three times by dispersing them in 0.5 ml PBS, and transferring the dispersions to new Eppendorf tubes. Proteins were desorbed from the particles by adding SDS (sodium dodecyl sulfate) and separated by SDS-PAGE. Negative controls with no particles were done for all protein conditions.

### *Dynamic Light Scattering (DLS)*

Dynamic light scattering data was obtained on a DynaPro PlateReader-II, Wyatt technologies, USA, using 10 or 20 seconds acquisition time and 10 acquisitions per sample. The data were analyzed with DynaPro software. The data was analysed by cumulants assuming monomodal size distribution and by regularization assuming multimodal size distribution. If the analyses fit equally well to the data we have used the number from the cumulant analyses. The data collected in 75% cow serum was corrected for the difference in viscosity.

### *Transmission electron microscopy (TEM)*

The samples were prepared by placing about 20  $\mu$ l of water at the surface of each sensor and removing the surface associated nanostructures from the substrate using the tip of the pipette. The nanostructures dispersed in water were sonicated for about 30 s to prevent agglomeration. Prior to analysis, TEM grids were dipped in the dispersions containing the nanostructures and left to dry on a tissue. TEM images were obtained

using a Tecnai T20 microscope (FEI, USA) with a LaB6 filament and an acceleration voltage of 200 kV. The size distribution of silica nanoparticles (n=59) was determined using Image J.

### **Decay length and bulk sensitivity factor determination**

The performance of the nanoplasmonic sensors, i.e. their bulk sensitivity factors ( $m$ ) and decay lengths ( $l_d$ ), were previously determined experimentally.<sup>1</sup> The bulk sensitivity factors (i.e. extinction peak shift ( $\Delta\lambda$ ) due to changes in bulk refractive index ( $n_{\text{medium}}$ )) were determined to 41, 104, and 206 nm per unit of refractive index for the 92, 123, and 167 nm nanostructures, respectively. Changes in bulk refractive index were achieved by using various concentrations (0-80%) of ethylene glycol.

To determine the decay lengths of the sensors, the extinction peak shifts were monitored after each step in a series of atomic layer depositions (ALD) of thin  $\text{Al}_2\text{O}_3$  films with varying thickness  $d$ . By fitting equation S1<sup>4</sup> to the observed response the decay lengths could be derived. For the three different sizes of the nanostructures the decay lengths were in the range of 9-35 nm in water and 11-51 nm in  $\text{N}_2$ , respectively, where the shortest decay length corresponds to the smallest nanostructure.

$$\Delta\lambda = m(n_{\text{layer}} - n_{\text{medium}})(1 - e^{-d/l_d}) \quad (\text{S1})$$

### **Normalization of corona formation kinetics data measured by NPS**

To be able to directly and quantitatively compare the rate of corona formation on the differently sized core-shell nanostructures we normalized the raw NPS data by their respective sensitivity factors (which are size dependent) derived from the NPS response to the deposition of a 5 nm thin (this thickness is comparable to a protein monolayer) *homogenous*  $\text{Al}_2\text{O}_3$  layer of. The  $\text{Al}_2\text{O}_3$  was deposited on all sensor structures by ALD using an Oxford FlexAl (Oxford Instruments, UK). For deposition of 5 nm  $\text{Al}_2\text{O}_3$ , 43 ALD cycles were run using trimethylaluminum as precursor. The deposited 5 nm oxide layer generated peak shifts of 5.5 nm, 7.9 nm, and 9.6 nm for the 92, 123, and 167 nm nanostructures, respectively, measured in an aqueous environment. By defining the response of the smallest nanostructures as the baseline, sensitivity factors used to normalize the NPS data could be determined as 1.00, 1.44, and 1.75 for the 92, 123, and 167 nm nanostructures, respectively. The normalized data of the corona formation kinetics are presented in Figure 3 in the main text. The corresponding raw data before sensitivity-factor-normalization are presented in Figure S4.

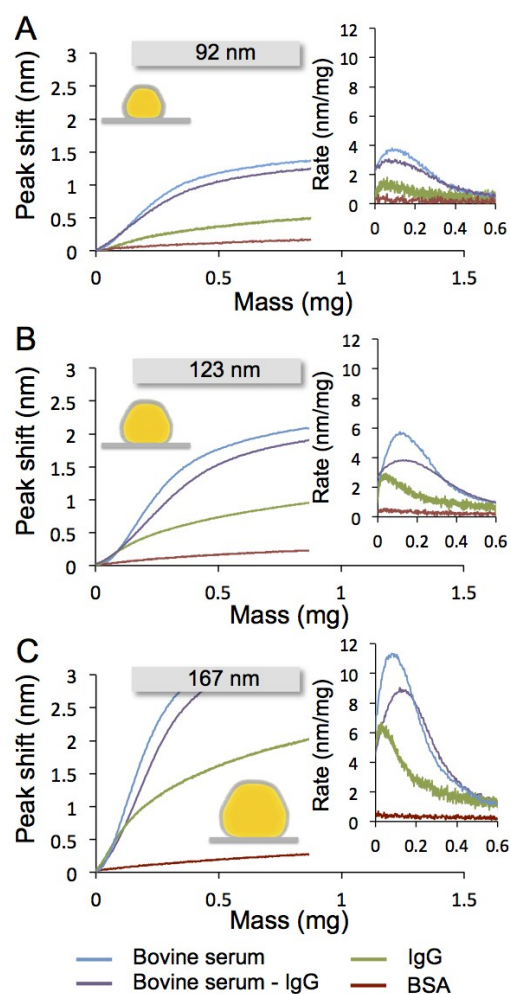


Figure S4. Kinetics of the corona formation (before normalization) upon addition of bovine serum, IgG depleted bovine serum (bovine serum - IgG), IgG and BSA using (A) 92 nm, (B) 123 nm and (C) 167 nm nanoplasmic sensors. The insets show the rate of adsorption during exposure for the first 0.6 mg of added protein.

### Summary of main results

A summary of the main results and their proposed interpretation are presented schematically in Figure S5. In the considered experiments both surface associated Au core - SiO<sub>2</sub> shell nanostructures (SiO<sub>2</sub> nanoparticle mimics) and dispersed SiO<sub>2</sub> nanoparticles were at first exposed to IgG or BSA. Upon exposure to IgG, the dispersed nanoparticles aggregate for all of the tested concentrations, while data obtained using differently sized core - shell nanostructures (i.e. different ratios between curved and flat regions) indicate that IgG adsorbs differently to flat and curved SiO<sub>2</sub> surfaces. The initial adsorption kinetics of IgG (and the serum samples) increased significantly with the size of the core-shell nanostructures, i.e. with an increased flat/curved ratio. These results encourage further studies aiming at determining the orientation of the IgG molecule. Upon exposure to BSA, the protein adsorbs to both types of nanomaterials, without inducing aggregation of the dispersed nanoparticles. In both cases, data of the corona thickness are obtained. It is important to note that DLS determines the increase in hydrodynamic diameter of the nanoparticles. Such increase may be independent of protein coverage. In contrast, the thickness calculated from the NPS data depends on the effective refractive index of the protein adlayer (i.e. the results depend on the surface

coverage of the protein). Observed thickness (dashed line) as a function of BSA coverage for both DLS and NPS are shown schematically in Figure S5, i.e. at low surface coverage the thickness calculated from the NPS data is smaller compared to the thickness determined by DLS.

In a second step, the BSA-precoated nanomaterials are exposed to a different biological sample (bovine serum or IgG). In these cases, the preadsorbed proteins are largely exchanged and a thicker corona is formed, as concluded from the combination of obtained NPS, DLS and SDS-PAGE results.

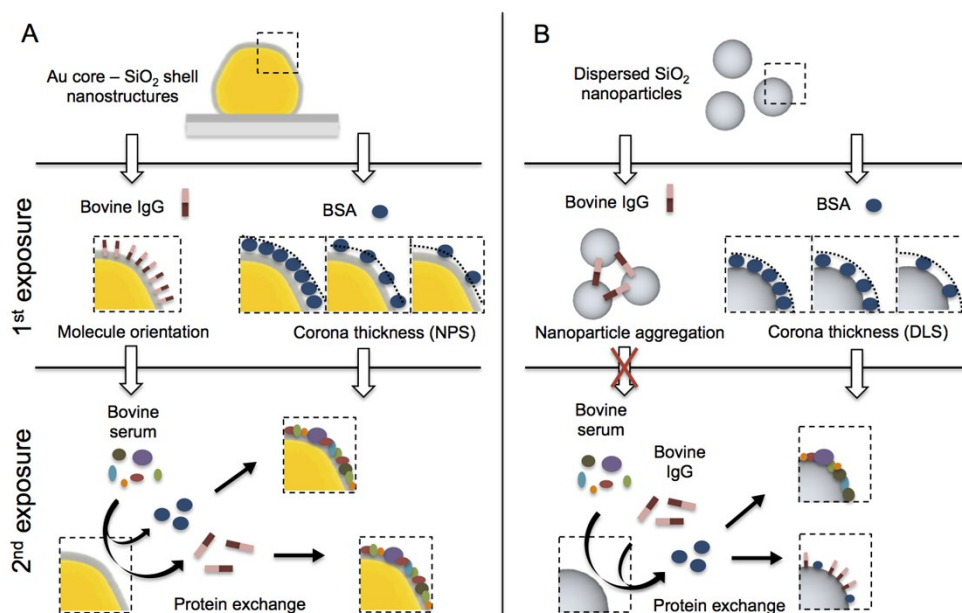


Figure S5. Schematic representation of selected results obtained using (A) Au core - SiO<sub>2</sub> shell nanostructures and NPS and (B) dispersed SiO<sub>2</sub> nanoparticles analyzed by DLS and SDS-PAGE. During a first exposure both types of nanomaterials were exposed to IgG or BSA. Upon exposure to IgG the NPS data indicated that IgG adsorbed with different orientations to flat and curved regions at the surface of the nanostructures, while the dispersed nanoparticles aggregated. Upon exposure to BSA a corona with a specific thickness was formed. For dispersed nanoparticles the thickness was analyzed using DLS (not sensitive to surface coverage) in contrast to the NPS data (sensitive to changes in RI and thus also to surface coverage), finding that the thickness determined by DLS corresponded well with a monolayer of BSA. During a second exposure, the core-shell nanostructures with a preformed IgG- or BSA-corona were exposed to bovine serum and the nanoparticles with a preformed BSA-corona were exposed to bovine serum or IgG. In all cases, the results showed that proteins from the new biological sample largely replaced the preadsorbed proteins.

## References

1. R. Frost, C. Wadell, A. Hellman, S. Molander, S. Svedhem, M. Persson and C. Langhammer, *ACS Sensors*, 2016, **1**, 798-806.
2. H. Fredriksson, Y. Alaverdyan, A. Dmitriev, C. Langhammer, D. S. Sutherland, M. Zaech and B. Kasemo, *Advanced Materials*, 2007, **19**, 4297-4302.
3. R. Cukalevski, S. A. Ferreira, C. J. Dunning, T. Berggard and T. Cedervall, *Nano Research*, 2015, **8**, 2733-2743.
4. O. Kedem, A. B. Tesler, A. Vaskevich and I. Rubinstein, *ACS Nano*, 2011, **5**, 748-760.